7.9

KINETIC MONTE CARLO METHOD TO MODEL DIFFUSION CONTROLLED PHASE TRANSFORMATIONS IN THE SOLID STATE

Georges Martin[1] and Frédéric Soisson[2]
[1]*Commissariat à l'Énergie Atomique, Cab. H.C., 33 rue de la Fédération, 75752 Paris Cedex 15, France*
[2]*CEA Saclay, DMN-SRMP, 91191 Gif-sur-Yuette, France*

The classical theories of diffusion-controlled transformations in the solid state (precipitate-nucleation, -growth, -coarsening, order-disorder transformation, domain growth) imply several *kinetic coefficients*: diffusion coefficients (for the solute to cluster into nuclei, or to move from smaller to larger precipitates...), transfer coefficients (for the solute to cross the interface in the case of interface-reaction controlled kinetics) and ordering kinetic coefficients. If we restrict to *coherent* phase transformations, i.e., transformations, which occur keeping the underlying lattice the same, all such events (diffusion, transfer, ordering) are nothing but jumps of atoms from site to site on the lattice. Recent progresses have made it possible to model, by various techniques, diffusion controlled phase transformations, in the solid state, starting from the jumps of atoms on the lattice. The purpose of the present chapter is to introduce one of the techniques, the Kinetic Monte Carlo method (KMC).

While the atomistic theory of diffusion has blossomed in the second half of the 20th century [1], establishing the link between the diffusion coefficient and the jump frequencies of atoms, nothing as general and powerful occurred for phase transformations, because of the complexity of the latter at the atomic scale. A major exception is ordering kinetics (at least in the homogeneous case, i.e., avoiding the question of the formation of microstructures), which has been described by the atomistic based Path Probability Method [2]. In contrast, supercomputers made it possible to simulate the formation of microstructures by just letting the lattice sites occupancy change in course of time following a variety of rules: the Kinetic Ising model (KIM) in particular has been (and

S. Yip (ed.),
Handbook of Materials Modeling, 2223–2248.

still is) extensively studied and is summarized in the appendix [3]; other models include "Diffusion Limited Aggregation", etc. . . Such models stimulate a whole field of the statistical physics of non-equilibrium processes. However, we choose here a distinct point of view, closer to materials science. Indeed, a unique skill of metallurgists is to master the formation of a desired microstructure simply by well controlled heat treatments, i.e., by imposing a strictly defined thermal history to the alloy. Can we model diffusion controlled phase transformations at a level of sophistication capable of reproducing the expertise of metallurgists?

Since Monte Carlo techniques were of common use in elucidating delicate points of the theory of diffusion in the solid state [4, 5], it has been quite natural to use the very same technique to simulate *diffusion controlled* coherent phase transformations. Doing so, one is certain to retain the full wealth that the intricacies of diffusion mechanisms might introduce in the *kinetic pathways* of phase transformations. In particular, the question of the time scale is a crucial one, since the success of a heat treatment in stabilizing a given microstructure, or in insuring the long-term integrity of that microstructure, is of key importance in Materials Science.

In the following, we first recall the physical foundation of the expression for the atomic jump frequency, we then recall the connection between jump frequencies and kinetic coefficients describing phase transformation kinetics; the KMC technique is then introduced and typical results pertaining to metallurgy relevant issues are given in the last section.

1. Jumps of Atoms in the Solid State

With a few exceptions, out of the scope of this introduction, atomic jump in solids is a thermally activated process. Whenever an atom jumps, say from site α to α', the configuration of the alloy changes from i to j. The probability per unit time, for the transition to occur, writes:

$$W_{i,j} = \nu_{i,j} \exp\left(-\frac{\Delta H_{i,j}}{k_B T}\right) \tag{1}$$

In Eq. (1), $\nu_{i,j}$ is the *attempt frequency*, k_B is the Boltzmann's constant, T is the temperature and $\Delta H_{i,j}$ is the *activation barrier* for the transition between configurations i and j. According to the rate theory [6], the attempt frequency writes, in the (quasi-) harmonic approximation:

$$\nu_{i,j} = \frac{\prod_{k=1}^{3N-3} \nu_k}{\prod_{k=1}^{3N-4} \nu'_k} \tag{2}$$

In Eq. (2), ν_k and ν'_k are the vibration eigen-frequencies of the solid, respectively in the initial configuration, i, and at the saddle point between configurations i and j. Notice that for a solid with N atoms, the number of eigen modes

is $3N$. However, the vibrations of the centre of mass (3 modes) are irrelevant in the diffusion process, hence the upper bound $3N-3$ in the product at the numerator. At the saddle point position between configurations i and j, one of the modes is a translation rather than a vibration mode, hence the upper bound $3N-4$ in the denominator.

Therefore, provided we know the value of $\Delta H_{i,j}$ and $\nu_{i,j}$ for each pair of configurations, i and j, we need to implement some algorithm which would propagate the system in its configuration space, as the jumps of atoms actually do in the real solid. Notice that the algorithm must be probabilistic since $W_{i,j}$ in Eq. (1) is a jump *probability* per unit time. Before we discuss this algorithm, we give some more details on diffusion mechanisms in solids, since the latter deeply affect the values of $W_{i,j}$ in Eq. (1).

The most common diffusion mechanisms in crystalline solids are vacancy-, interstitial- and interstitialcy-diffusion [7].

Vacancies (a vacant lattice site) allow for the jumps of atoms from site to site on the lattice; in alloys, vacancy diffusion is responsible for the migration of solvent- and of substitutional solute- atoms. Therefore, the transition from configuration i to j implies that one atom and one (nearest neighbor) vacancy exchange their position. As a consequence, the higher the vacancy concentration, the more numerous are the configurations, which can be reached from configuration i: indeed, starting from configuration i, any jump of any vacancy destroys that configuration. Therefore the transformation rate depends both on the jump frequencies of vacancies, as given by Eq. (1), and on the concentration of vacancies in the solid. This fact is commonly taken advantage of, in practical metallurgy. At equilibrium, the vacancy concentration depends on the temperature, the pressure and, in alloys, of the chemical potential differences between the species:

$$C_v^e = \exp\left(-\frac{g_v^f}{k_B T}\right) \tag{3}$$

In Eq. (3), $C_v^e = N_v/(N + N_v)$, with N the number of atoms, and g_v^f is the free enthalpy of formation of the vacancy. At equilibrium, the probability for an atom to jump equals the product of the probability for a vacancy to be nearest neighbor of that atom (deduced from Eq. 3), times the jump frequency given by Eq. (1). In real materials, vacancies form and annihilate at lattice discontinuities (free surfaces, dislocation lines and other lattice defects). If, in course of the phase transformation the equilibrium vacancy concentration changes, e.g., because of vacancy trapping in one of the phases, it takes some time for the vacancy concentration to adjust to its equilibrium value. This point, of common use in practical metallurgy, is poorly known from the basic point of view [8] and will be discussed later.

Interstitial diffusion occurs when an interstitial atom (like carbon or nitrogen in steels) jumps to a nearest neighbor unoccupied interstitial site.

Interstitialcy diffusion mechanism implies that a substitutional atom is "pushed" into an interstitial position by a nearest neighbor interstitial atom, which itself, becomes a substitutional one. This mechanism prevails, in particular, in metals under irradiation, where the collisions of lattice atoms with the incident particles produce Frenkel pairs; a Frenkel pair is made of one vacancy and one dumb-bell interstitial (two atoms competing for one lattice site). The migration of the dumb-bell occurs by the interstitialcy mechanism. The concentration of dumb-bell interstitials results from the competition between the production of Frenkel pairs by nuclear collisions and of their annihilation either by recombination with vacancies or by elimination on some lattice discontinuity. The interstitialcy mechanism may also prevail in some ionic crystals, and in the diffusion of some gas atoms in metals.

2. From Atomic Jumps to Diffusion and to the Kinetics of Phase Transformations

The link between the jump frequencies and the diffusion coefficients has been established in details in limiting cases [1]. The expressions are useful for adjusting the values of the jump frequencies to be used, to experimental data. As a matter of illustration, we give below some expressions for the vacancy diffusion mechanism in crystals with cubic symmetry (with a for the lattice parameter):

– In a pure solvent, the tracer diffusion coefficient writes:

$$D^* = a^2 f_0 W_0 C_v^e, \tag{4a}$$

with f_0 for the correlation factor (a purely geometrical factor) and W_0, the jump frequency of the vacancy in the pure metal.

– In a dilute solution with Face Centered Cubic (FCC) lattice, with non interacting solutes, and assuming that the spectrum of the vacancy jump frequencies is limited to 5 distinct values (W_i, $i = 0$ to 4, for the vacancy jumps respectively in the solvent, around one solute atom, toward the solute, toward a solvent atom nearest neighbor of the solute, and away from the solute atom, see Fig. 1), the solute diffusion coefficient writes:

$$D_{\text{solute}} = a^2 C_v^e \frac{W_4}{W_3} f_2 W_2, \tag{4b}$$

where the correlation factor f_2 can be expressed as a function of the W_i's. In dilute solutions, the solvent- as well as the solute-diffusion coefficient depends linearly on the solute concentration, C, as:

$$D^*(C) = D^*(0)(1 + bC). \tag{4c}$$

The expression of b is given in [1, 9].

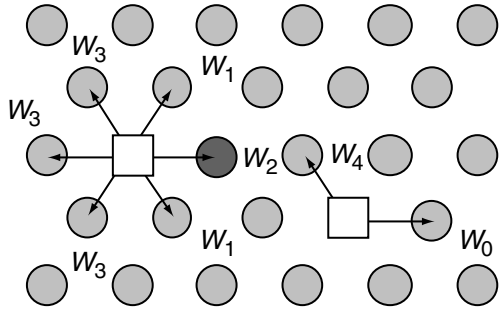

Figure 1. The Five-frequency model in dilute FCC alloys: the five types of vacancy jumps are represented in a (111) plane (light gray: solvent atoms, dark gray: solute atom, open square: vacancies).

– In concentrated alloys, approximate expressions have been recently derived [10].

The atomistic foundation of the classical models of diffusion controlled coherent phase transformation is far less clear. For precipitation problems, two main techniques are of common use: the nucleation theory (and its atomistic variant sometimes named "cluster dynamics") and Cahn–Hilliard diffusion equation [11].

In the nucleation theory, one defines the formation free energy (or enthalpy, if the transformation occurs under fixed pressure), $F(R)$ of a nucleus with size R (volume vR^3 and interfacial area sR^2, v and s being geometric factors computed for the equilibrium shape):

$$F(R) = \delta\mu vR^3 + \sigma sR^2. \tag{5}$$

In Eq. (5), $\delta\mu$ and σ are respectively the gain of chemical potential on forming one unit volume of second phase, and the interfacial free energy (or free enthalpy) per unit area. If the solid solution is supersaturated, $\delta\mu$ is negative and $F(R)$ first increases as a function of R, then goes through a maximum for the critical size R^* ($R^* = (2s/3v)\,(\sigma/|\delta\mu|)$) and then decreases (Fig. 2). $F(R)$ can be given a more precise form, in particular for small values of R. More details may be found in Perini *et al.* [12].

For the critical nucleus,

$$F^* = F(R^*) \approx \sigma^3/(\delta\mu)^2. \tag{6}$$

$F(R)$ can be seen as an energy hill which opposes the growth of sub-critical nuclei ($R < R^*$) and which drives the growth of super-critical nuclei ($R > R^*$). The higher the barrier, i.e., the larger F^*, the more difficult the nucleation is. F^* is very sensitive to the gain in chemical potential: the higher the supersaturation, the larger the gain, the shallower the barrier, and the easier the

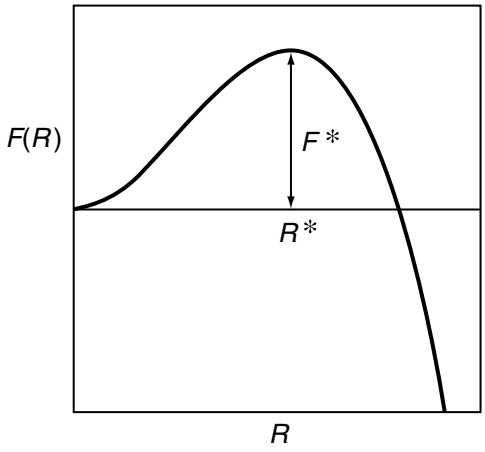

Figure 2. Free energy change on forming a nucleus with radius R.

nucleation. F^* also strongly depends on the interfacial energy, a poorly known quantity, which, in principle depends on the temperature.

With the above formalism, the nucleation rate (i.e., the number of supercritical nuclei which form per unit time in a unit volume) writes, under stationary conditions:

$$J_{\text{steady}} = \beta^* Z N_0 \exp\left(-\frac{F^*}{k_B T}\right) \tag{7a}$$

with N_0 for the number of lattice sites and Z for the Zeldovich's constant:

$$Z = \left[-\frac{1}{2\pi kT}\left(\frac{\partial^2 F}{\partial n^2}\right)_{n=n^*}\right]^{1/2}, \tag{7b}$$

n for the number of solute atoms in a cluster and θ^* for the sticking rate of solute atoms on the critical nucleus. If the probability of encounter of one solute atom with one nucleus is diffusion controlled:

$$\beta(R) = 4\pi DRC \tag{7c}$$

For a detailed discussion, see Waite [13]. In Eq. (7c), D is the *solute diffusion coefficient* in the (supersaturated) matrix with the solute concentration C.

An interesting quantity is the incubation time for precipitation, τ_{inc}, i.e., the time below which the nucleation current is much smaller than J_{steady}. The former writes:

$$\tau_{\text{inc}} \propto \frac{1}{\beta^* Z^2} \tag{7d}$$

When the supersaturation is small and/or the interfacial energy is high, the incubation time gets very large. Also the incubation time is scaled to the diffusion coefficient of the solute.

The nucleation process can be described also by the technique named "cluster dynamics". The microstructure is described, at any time, by the number density, ρn, of clusters made of n solute atoms. The latter varies in time as:

$$\frac{\mathrm{d}\rho_n}{\mathrm{d}t} = -\rho_n(\alpha_n + \beta_n) + \rho_{n+1}\alpha_{n+1} + \rho_{n-1}\beta_{n-1} \tag{8}$$

where α_n and β_n are respectively the rate of solute evaporation and sticking at a cluster of n solute atoms. Again, α_n and β_n can be expressed in terms of solute diffusion or transfer coefficients.

At later stages, when the second phase precipitation has exhausted the solute supersaturation, Ostwald ripening takes place: because the chemical potential of the solute close to a precipitate increases with the curvature of the precipitate-matrix interface ($\delta\mu(R) = 2\sigma/R$), the smaller precipitates dissolve to the benefit of the larger ones. According to Lifschitz and Slyosov and to Wagner [14], the mean precipitate volume increases linearly with time, or the mean radius (as well as the mean precipitate spacing) goes as:

$$R(t) - R(0) = k\, t^{1/3} \tag{9a}$$

with

$$k^3 = \frac{(8/9) D\sigma\Omega C_s}{k_\mathrm{B} T} \tag{9b}$$

In Eq. (9b), D is again the solute diffusion coefficient, C_s the solubility limit, and Ω the atomic volume. The problem of multicomponent alloys has been addressed by several authors [15].

The above models do not actually generate a full microstructure: they give the size distribution of precipitates as a function of time, as well as the mean precipitate spacing, since the total amount of solute is conserved, provided that the precipitates do not change composition in the course of the phase separation process.

The formation of a full microstructure (i.e., including the variability of precipitate shapes, the correlation in the positions of precipitates etc.) is best described by Cahn's diffusion equation [16]. In the latter, the chemical potential, the gradient of which is the driving force for diffusion, includes an inhomogeneity term, i.e., is a function, at each point, both of the concentration and of the curvature of the concentration field. The diffusion coefficient was originally given the form due to Darken. Based on a simple model of $W_{i,j}$ and a mean field approximation, an atomistic based expression of the mobility has been proposed, both for binary [17] and multicomponent alloys [18]. When precipitation occurs together with ordering, Cahn's equation is complemented with an equation for the relaxation of the degree of order; the latter relaxation occurs at a rate proportional to the gain in free energy due to the onsite relaxation of the degree order. The rate constant is chosen arbitrarily [19]. Since in a crystalline

sample the ordering reaction proceeds by the very same diffusion mechanism as the precipitation, both rate constants (for the concentration- and for the degree of order fields) should be expressed from the same set of $W_{i,j}$. This introduces some couplings, which have been ignored by classical theories [20].

As a summary, despite their efficiency, the theories of coherent phase separation introduce rate constants (diffusion coefficients, interfacial transfer coefficients, rate constants for ordering) the microscopic definition of which is not fully settled.

The KMC technique offers a means to by-pass the above difficulties and to directly simulate the formation of a microstructure in an alloy where atoms jump with the frequencies defined by Eq. (1).

3. Kinetic Monte Carlo Technique to Simulate Coherent Phase Transformations

The KMC technique can be implemented in various manners. The one we present here has a transparent physical meaning.

3.1. Algorithm

Consider a computational cell with N_s sites, N_a atoms and $N_v = N_s - N_a$ vacancies; each lattice site is linked to Z neighbor sites with which atoms may be exchanged (usually, but not necessarily, nearest neighbor sites). A configuration is defined by the labels of the sites occupied respectively by A, B, C, ... atoms and by vacancies. Each configuration "i" can be escaped by N_{ch} channels ($N_{ch} = N_v Z$ minus the number of vacancy–vacancy bounds if any), leading to N_{ch} new configurations "j_1" to "j_{Nch}". The probability that the transition "$i; j_q$" occurs per unit time is given by Eq. (1) which can be computed a priori provided a model is chosen for $\Delta H_{i,j}$ and $\nu_{i,j}$. Since the configuration "i" may disappear by N_{ch} independent channels, the probability for the configuration to disappear per unit time, W_i^{out}, is the sum of the probabilities it decays by each channel ($W_{i,jq}$, $q = 1$ to N_{ch}), and the life time τ_i of the configuration is the inverse of W_i^{out}:

$$\tau_i = \left(\sum_{q=1}^{N_{ch}} W_{i,j_q} \right)^{-1} \tag{10a}$$

The probability that the configuration "j_q" is reached among the N_{ch} target configurations is simply given by:

$$P_{ij_q} = \frac{W_{i,j_q}}{\sum\limits_{q=1}^{N_{ch}} W_{i,j_q}} = W_{i,j_q} \times \tau_i \tag{10b}$$

Assuming all possible values of W_{i,j_q} are known (see below), the code proceeds as follows:

Start at time $t = 0$ from the configuration "i_0", set $i = i_0$;

1. Compute τ_i (Eq. (10a)) and the N_{ch} values of $S_{i,k} = \sum_{q=1}^{k} P_{ij_q}$, $k = 1$ to N_{ch}.
2. Generate a random number R on]0; 1].
3. Find the value of f to be given to k such that $S_{i,k-1} < R \leq S_{i,k}$. Choose f as the final configuration.
4. Increment the time by $\tau_i (t_{MC} => t_{MC} + \tau_i)$ and repeat the process from step 1, giving to i the value f.

3.2. Models for the Transition Probabilities $W_{i,j}$ (Eq. (1))

For a practical use of the above algorithm, we need a model for the transitions probabilities per unit time, $W_{i,j}$. In principle, at least, given an interatomic potential, all quantities appearing in Eqs. (1)–(3) can be computed for any pair of configurations, hence $W_{i,j}$. The computational cost for this is so high that most studies use simplified models for the parameters entering Eqs. (1)–(3); the values of the parameters are obtained by fitting appropriate quantities to available experimental data, such as phase boundaries and tie lines in the equilibrium phase diagram, vacancy formation energy and diffusion coefficients. We describe below the most commonly used models, starting from the simplest one.

Model (a) The energy of any configuration is a sum of pair interactions ε with a finite range (nearest- or farther neighbors). The configurational energy is the sum of the contributions of two types of bounds: those which are modified by the jump, and those which are not. We name e_{sp} the contribution of the bounds created in the saddle point configuration. This model is illustrated in Fig. 3. The simplest version of this model is to assume that e_{sp} depends neither on the atomic species undergoing the jump, nor on the composition in the surrounding of the saddle point [17].

Model (b) Same as above, but with e_{sp} depending on the atomic species at the saddle point. This approximation turned out to be necessary to account for the contrast in diffusivities in the ternary Ni–Cr–Al [21].

Model (c) Same as above, but with e_{sp} written as a sum of pair interactions [22]. This turned out to provide an excellent fit to the activation barriers computed in Fe(Cu) form fully relaxed atomistic simulations based on an EAM potential. As shown on Fig. (4), the

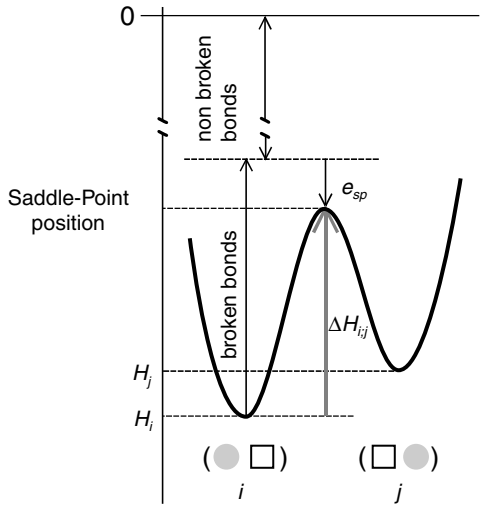

Figure 3. Computing the migration barrier between configurations i and j (Eq. (1)), from the contribution of broken- and restored bounds.

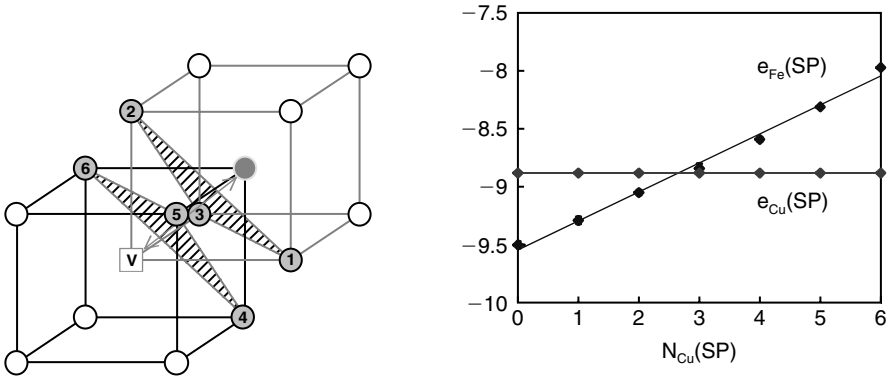

Figure 4. The six nearest-neighbors (labeled 1 to 6) of the saddle-point in the BCC lattice (left). Contribution to the configurational energy, of one Fe atom, e_{Fe}(SP), or one Cu atom, e_{Cu}(SP), at the saddle point, as a function of the number of Cu atoms nearest neighbor of the saddle point (right).

contribution to the energy of one Cu atom at the saddle point, $\mathrm{e_{Cu}}$(SP), does not depend on the number of Cu atoms around the saddle point, while that of one Fe atom, $\mathrm{e_{Fe}}$(SP), increases linearly with the latter.

Model (d) The energy of each configuration is a sum of pair and multiple interactions [18]. Taking into account higher order interactions permits to reproduce phase diagrams beyond the regular solution

model. The attempt frequency (Eq. 2) was adjusted, based on an empirical correlation between the pre-exponential factor and the activation enthalpy. Complex experimental interdiffusion profiles in four components alloys (AgInCdSn) could be reproduced successfully. Multiplet interactions have been used in KMC to model phase separation and ordering in AlZr alloys [23].

Model (e) The energies of each configuration and at the saddle point, as well as the vibration frequency spectrum (entering Eq. (2)) are computed from a many body interaction potential [24]. The vibration frequency spectrum can be estimated either with Einstein's model [25] or Debye approximation [26, 27].

The above list of approximations pertains to the vacancy diffusion mechanism. Fewer studies imply also interstitial diffusion, as carbon in iron, or dumbbell diffusion, in metals under irradiation, as will be seen in the next section. The models for the activation barrier are of model (b) described above.

3.3. Physical Time and Vacancy Concentration

Consider the vacancy diffusion mechanism. If the simulation cell only contains one vacancy, the vacancy concentration is $1/N_s$, often much larger than a typical equilibrium vacancy concentration C_v^e. From Eq. (10), we conclude that the time evolution in the cell is faster than the real one, by a factor equal to the vacancy supersaturation in the cell: $(1/N_s)/C_v^e$. The physical time, t is therefore longer than the Monte Carlo time, t_{MC}, computed above:

$$t = t_{\mathrm{MC}}/(N_s C_v^e) \tag{11}$$

Equation (11) works as long as the equilibrium vacancy concentration does not vary much in the course of the phase separation process, a point which we discuss now.

Consider an alloy made of N_A atoms A, N_B atoms B on N_s lattice sites. For any atomic configuration of the alloy, there is an optimum number of lattice sites, N_s^e, that minimizes the configurational free energy; the vacancy concentration in equilibrium with that configuration is: $C_v^e = (N_s^e - N_A - N_B)/N_s^e$. For example assume that the configurations can be described by K types of sites onto which the vacancy is bounded by an energy E_{bk} ($k = 1$ to K), with $k = 1$ corresponding to sites surrounded by pure solvent ($E_{b1} = 0$). We name $N_1, \ldots, N_K$ the respective numbers of such sites. The equilibrium concentrations of vacancies on the sites of type 1 to K are respectively:

$$C_{vk}^e = \frac{N_{vk}}{N_k + N_{vk}} = \exp\left(-\frac{E_f + E_{bk}}{k_{\mathrm{B}} T}\right) \tag{12a}$$

In Eq. (11), E_f is the formation energy of a vacancy in pure A. The total vacancy concentration, in equilibrium with the configuration as defined by $N_1, \ldots, N_K$ is thus (in the limit of small vacancy concentrations):

$$C_v^e \approx \frac{\sum_k N_k C_{vk}^e}{\sum_k N_k} = C_{v0}^e \left(\frac{1 + \sum_{k=2,K} X_k \exp(-E_{bk}/k_B T)}{1 + \sum_{k=2,K} X_k} \right);$$
$$X_k = N_k / N_1 \tag{12b}$$

In Eq. (12), C_{v0}^e is the equilibrium vacancy concentration in the pure solvent, and X_k depends on the advancement of the phase separation process: e.g., in the early stages of solute clustering, we expect the proportion of sites surrounded by a small number of solute atoms to decrease. The overall vacancy equilibrium concentration thus changes in time (Eq. (12b)), while it remains unaffected for each type of site (Eq. (12a)). Imposing a fixed number of vacancies in the simulation cell, creates the opposite situation: in the simulation, the *overall* vacancy concentration is kept constant, thus the vacancy *concentration on each type of site* must change in course of time: the kinetic pathway will be altered.

This problem can be faced in various ways. We quote below two of them:

- *Rescaling the time from an estimate of the free vacancy concentration*, i.e., the concentration of those vacancies with no solute as neighbor [22]. The vacancy concentration in the solvent is estimated in the course of the simulation, at a certain time scale, Δt, from the fraction of the time, where the vacancy is surrounded by solvent atoms only. Each time interval Δt is rescaled by the vacancy super saturation, which prevails during that time interval.
- *Modeling a vacancy source* (*sink*) *in the simulation cell* [28]: in real materials, vacancies are formed and destroyed at lattice discontinuities (extended defects), such as dislocation lines (more precisely jogs on the dislocation line), grain boundaries, incoherent interfaces and free surfaces. The simplest scheme is as follows: creating one vacancy implies that one atom on the lattice close to the extended defect jumps into the latter in such a way as to extend the lattice by one site; eliminating one vacancy implies that one atom at the extended defect jumps into the nearby vacancy. Vacancy formation and elimination are a few more channels by which a configuration may change. The transition frequencies are still given by Eq. (1) with appropriate activation barriers: Fig. 5 gives a generic energy diagram for the latter transitions.

As shown by the above scheme, while the vacancy equilibrium concentration is dictated by the formation energy, E_f, the time to adjust to a change in the equilibrium vacancy concentration implies the three parameters E_f,

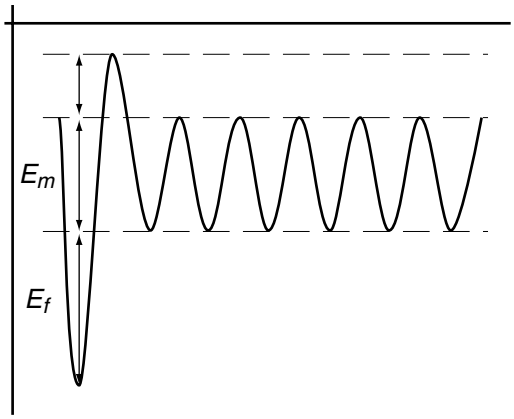

Figure 5. Configurational energy as a function of the position of the vacancy. When one vacancy is added to the crystal, the energy is increased by E_f.

E_m and δ. In other words, a given equilibrium concentration can be achieved either by *frequent* or by *rare* vacancy births and deaths. The consequences of this fact on the formation of metastable phases during alloy decomposition are not yet fully understood.

3.4. Tools to Characterize the Results

The output of a KMC simulation is a string of atomistic configurations as a function of time. The latter can be observed by the eye (e.g., to recognize specific features in the shape of solute clusters); one can also measure various characteristics (short range order, cluster size distribution, cluster composition and type of ordering...); one can simulate signals one would get from classical techniques such as small- or large-angle scattering, or use the very same tools as used in Atom Probe Field Ion Microscopy to process the very same data, namely the location of each type of atom. Some examples are given below.

3.5. Comparison with the Kinetic Ising Model

The KIM, of common use in the Statistical Physics community, is summarized in the appendix. It is easily checked that the models presented above for the transition probabilities introduce new features, which are not addressed by the KIM. In particular, the only energetic parameter to appear in KIM is what is named, in the community of alloys thermodynamics, the ordering energy: $\omega = \varepsilon_{AB} - (\varepsilon_{AA} + \varepsilon_{BB})/2$ (for the sake of simplicity, we restrict, here, to two

component alloys). While ω is indeed the only parameter to enter equilibrium thermodynamics, the models we introduced show that the kinetic pathways are affected by a second independent energetic parameter, the asymmetry between the cohesive energies of the pure elements: $\varepsilon_{AA} - \varepsilon_{BB}$. This point is discussed into details, by Athènes and coworkers [29–31]. Also, the description of the activated state between two configurations is more flexible in the present model as compared to KIM. For these reasons, the present model offers unique possibilities to study complex kinetic pathways, a common feature in real materials.

4. Typical Results: What has been Learned

In the 70s the early KMC simulations have been devoted to the study of simple ordering and phase separation kinetics in binary systems with conserved or non-conserved order parameters. Based on the Kinetic Ising model and so called "Kawazaki dynamics" (direct exchange between nearest neighbor atoms, with a probability proportional to $\exp[-(H_{\text{final}} - H_{\text{initial}})/2k_{\text{B}}T]$), with no point defects and no migration barriers, they could mainly reproduce some generic features of intermediate time behaviors, taking the number of Monte Carlo step as an estimate of physical time: the coarsening regime of precipitation with $R - R_0 \propto t^{1/3}$; the growth rate of ordered domains $R - R_0 \propto t^{1/2}$, dynamical scaling laws, etc. [3, 32]. However, such models cannot reproduce important metallurgical features such as the role of distinct solute and solvent mobilities, of point defect trapping, or of correlations among successive atomic jumps etc. In the frame of the models (a)–(e) previously described, these features are mainly controlled by the asymmetry parameters for the stable configuration- and saddle-point energies (respectively $\varepsilon_{AA} - \varepsilon_{BB}$, and $e_A^{\text{sp}} - e_B^{\text{sp}}$). We give below typical results, which illustrate the sensitivity, to the above features, of the kinetic pathways of phase transformations.

4.1. Diffusion in Ordered Phases

Since precipitates are often ordered phases, the ability of the transition probability models to well describe diffusion in ordered phases must be assessed. As an example, diffusion in B2 ordered phases presents specific features which have been related to the details of the diffusion mechanism: at a given composition, the Arrhenius plot displays a break at the order/disorder temperature and an upward curvature in the ordered phase; at a given temperature, the tracer diffusion coefficients are minimum close to the stoichiometric composition. The reason for that is as follows: starting from a perfectly

ordered B2 phase, any vacancy jump creates an antisite defect, so that the most probable next jump is the reverse one which annihilates the defect. As a consequence, it has been proposed that diffusion in B2 phases occurs via highly correlated vacancy jump sequences, such as the so-called 6-jump cycle (6JC) which corresponds to 6 *effective* vacancy jumps (resulting from many more jumps, most of them being canceled by opposite jumps).

Based on the above "model (a)" for the jump frequency, Athènes' KMC simulations [29] show that other mechanisms (e.g., the antisite-assisted 6JC) contribute to long-range diffusion, in addition to the classical 6JC (see Figure 6). Their relative importance increases with the asymmetry parameter $u = \varepsilon_{AA} - \varepsilon_{BB}$, which controls the respective vacancy concentrations on the two B2 sublattices and the relative mobilities of A and B atoms. Moreover while diffusion by 6JC only would implies a D_A^*/D_B^* ratio between $1/2$ and 2, the newly discovered antisite-assisted cycles yield to a wider range, as observed experimentally in some B2 alloys, such as Co–Ga. Moreover, high asymmetry parameters produce an upward curvature of the Arrhenius plot in the B2 domain. Similar KMC model has been applied to the $L1_2$ ordered structures and successfully explains some particular diffusion properties in these phases [30].

4.2. Simple Unmixing: Iron–Copper Alloys

Copper precipitation in α-Fe has been extensively studied with KMC: although pure copper has an FCC structure, experimental observations show that the first step of precipitation is indeed fully coherent, up to precipitate radii of the order of 2 nm, with a Cu BCC lattice parameter very close to that of iron. The composition of the small BCC copper clusters has long been debated: early atom probe or field ion microscopy studies or small angle neutron scattering experiments suggested that they might contain more than 50%

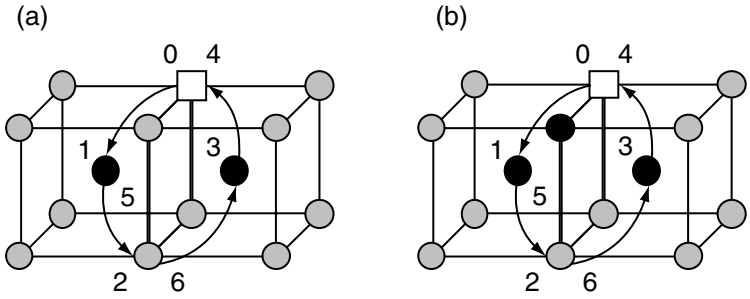

Figure 6. Classical Six Jump Cycle (a) and Antisite assisted Six Jump Cycle (b) in B2 compounds [29].

iron, while others experimental techniques suggested pure copper clusters. Using the above simple "model (a)", KMC suggest almost pure copper precipitates, but with very irregular shapes [33]: the significant iron content measured in some experiments could then be due to the contribution of atoms at the precipitate matrix interface if a simple smooth shape is attributed to the precipitate while the small Cu clusters have very irregular shapes. This explanation is in agreement with the most direct observations using a 3D atom probe [34]. The simulations have also shown that, with the parameter values we used, fast migration of small Cu clusters occurs: the latter induces direct coagulation between nuclei, yielding ramified precipitate morphologies.

On the same Fe–Cu system, Le Bouar and Soisson [22] have used an EAM potential to parameterize the activation barriers in Eq. (1). In dilute alloys, the EAM computed energies of stable and saddle-point relaxed configurations, can be reproduced with pair interactions on a rigid lattice (including some vacancy-atom interactions). The saddle-point binding energies of Fe and Cu are shown in Fig. 4 and have already been discussed. Such a dependence of the SP binding energies does not modify the thermodynamic properties of the system (the solubility limit, the precipitation driving force, the interfacial energies, the vacancy concentrations in various phases do not depend on the SP properties) and it slightly affects the diffusion coefficients of Fe and Cu in pure iron. Nevertheless such details strongly affect the precipitation kinetic pathway, by changing the diffusion coefficients of small Cu clusters and thus the balance between the two possible growth mechanisms: classical emission-adsorption of single solute atoms and direct coagulation between precipitates. This is illustrated by Fig. 7, where two simulations of copper precipitation are displayed: one which takes into account the dependence of e_{sp}^{Fe} on the local atomic composition and one with a constant e_{sp}^{Fe}. In the second case small copper clusters (with typically less than 10 Cu atoms) are more mobile than in the first case, which results in an acceleration of the precipitation. Moreover, the nucleation regime in Fig. 7(b) almost vanishes, because two small clusters can merge as- or even more rapidly than a Cu monomer and a precipitate. The dashed line of Fig. 7 represents the results obtained with the empirical parameter values described in the previous paragraph [33]: as can be seen these results do not differ qualitatively from those obtained by Le Bouar *et al*. [22], so that the qualitative interpretation of the experimental observations is conserved.

The competition between the classical solute emission–adsorption and direct precipitate coagulation mechanisms observed in dilute Fe–Cu alloys appears indeed to be quite general and to have important consequences on the whole kinetic pathway. First studies [35] focused on the role of the atomic jump mechanism (Kawasaki dynamics versus vacancy jump), but recent KMC simulations based on the transition probability models (a)–(c) above have shown that both single solute atom- and cluster-diffusion are observed when

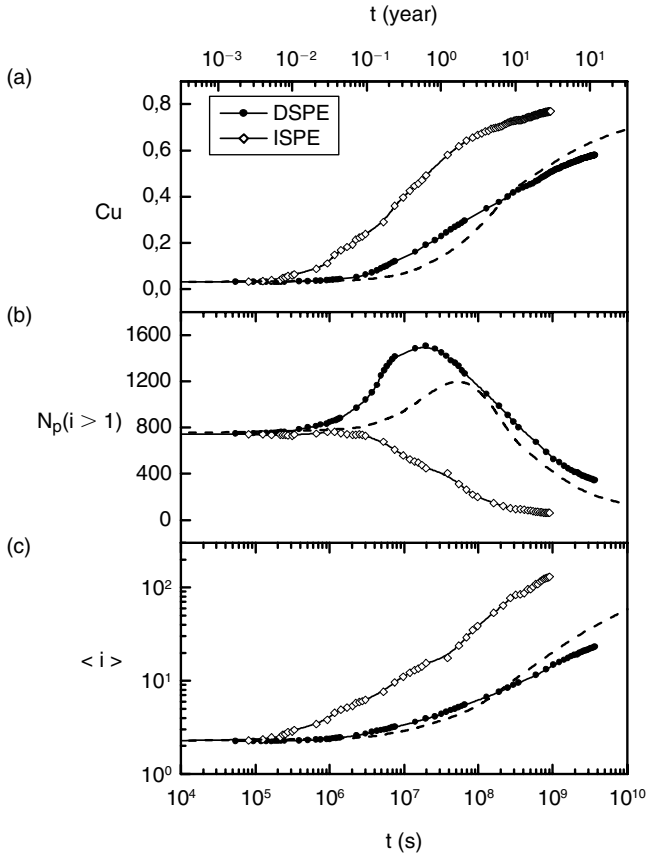

Figure 7. Precipitation kinetics in a Fe-3at.%Cu alloy at T = 573 K [22]. Evolution of (a) the degree of the copper short-range order parameter, (b) the number of supercritical precipitates and (c) the averaged size of supercritical precipitates. Monte Carlo simulations with e_{sp}^{Fe} depending on the local atomic configuration (•) or not (◇). The dashed lines corresponds to the results of Soisson *et al*. [33].

vacancy diffusion is carefully modeled. Indeed the balance between both mechanisms is controlled by:

– the asymmetry parameter which controls the relative vacancy concentrations in the various phases [31]. A vacancy trapping in the precipitates (e.g., in Fe–Cu alloys) or at the precipitate-matrix interface tends to favor direct coagulation, while if the vacancy concentration is higher in the matrix, as is the case for Co precipitation in Cu, [36], the migration of monomers and emission-adsorption of single solute atoms are dominant.

– the saddle-point energies which, together with the asymmetry parameter, control the correlation between successive vacancy jumps and the migration of solute clusters [22].

4.3. Nucleation/Growth/Coarsening: Comparison with Classical Theories

The classical theories of nucleation, growth or coarsening, as well as the theory of spinodal decomposition in highly supersaturated solid solutions, can be assessed using KMC simulations [37]. For the nucleation regime, the thermodynamic and kinetic data involved in Eqs. (5)–(7) (the driving force for precipitation, $\delta\mu$, the interfacial energy, σ, the adsorption rate β, etc.) can be computed from the atomistic parameters used in KMC (pair interaction, saddle-point binding energies, attempt frequencies): a direct assessment of the classical theories is thus possible. For low supersaturations and in cases where only the solute monomers are mobile, the incubation time and the steady–state nucleation rate measured in the KMC simulations are very close to those predicted by the classical theory of nucleation. On the contrary, when small solute clusters are mobile (keeping the overall solute diffusion coefficient the same), the classical theory strongly overestimates the incubation time and weakly underestimates the nucleation rate, as exemplified on Fig. 8.

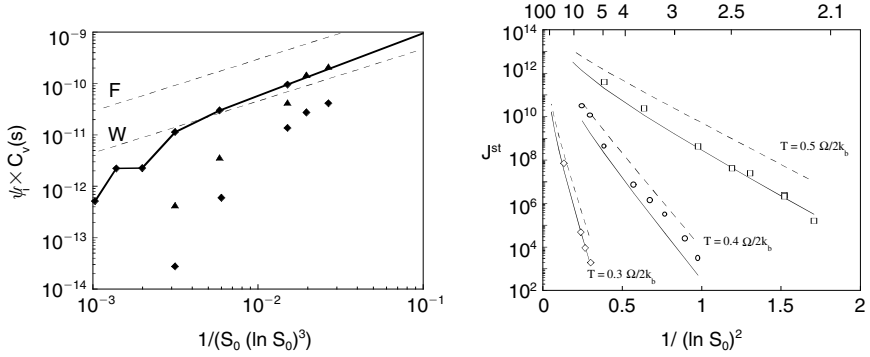

Figure 8. Incubation time and steady-state nucleation rate, in a binary model alloy A–B, as a function of supersaturation $S_0 = C_B^0/C_B^{eq}$ (initial/equilibrium B concentration in the solid solution). Comparison of KMC (symbols) and Classical Theory of Nucleation (lines). On the left: the dotted lines refer to two classical expressions of the incubation time (Eq. (7d)), the plain line is obtained by numerical integration of Eq. (8); ▲ KMC with mobile monomers only, ♦ KMC with small mobile clusters. On the right: the dotted and plain lines refer to Eq. (7a) with respectively $Z = 1$ or Z from Eq. (7b); ◇, ○ and □ refer to KMC with mobile monomers. For more details, see Ref. [37].

The above general argument has been assessed in the case of Al_3Zr and Al_3Sc precipitation in dilute aluminum alloys: the best estimates of the parameters suggest that diffusion of Zr and Sc in Al occurs by monomer migration [38]. When the precipitation driving force and interfacial energy are computed in the frame of the Cluster Variation Method, the classical theory of nucleation predicts nucleation rates in excellent agreement with the results of the KMC simulations, for various temperatures and supersaturations. Similarly, the distribution of cluster sizes in the solid solution $\rho_n \sim \exp(-F_n/k_B T)$, with F_n given by the capillarity approximation (Eq. (5)) is well reproduced, even for very small precipitate sizes.

4.4. Precipitation in Ordered Phases

The kinetic pathways become more complex when ordering occurs in addition to simple unmixing. Such kinetics have been explored by Athènes [39] in model BCC binary alloys, in which the phase diagram displays a tricritical point and a two-phase field (between a solute rich B2 ordered phase and a solute depleted A2 disordered phase). The simulation was able to reproduce qualitatively the main experimental features reported from transmission electron microscopy observations during the decomposition of Fe–Al solid solutions:

(i) for small supersaturations, a nucleation-growth-coarsening sequence of small B2 ordered precipitates in the disordered matrix occurs;
(ii) for higher supersaturations, a short range ordering starts before any modification of the composition field, followed by a congruent ordering with a very high density of antiphase boundaries (APB). In the center of the two phase field, this homogeneous state then decomposes by a thickening of the APBs which turns into the A2 phase. Close to the B2 phase boundary, the decomposition process also involves a nucleation of iron rich A2 precipitates inside the B2 phase.

Varying the asymmetry parameter u mainly affects the time scale. However qualitative differences are observed, at very early stages, in the formation of ordered microstructures: if the value of u enhances preferentially the vacancy exchanges with the majority atoms ($u > 0$), ordering proceeds everywhere, in a diffuse manner; while if u favors vacancy exchanges with the solute atoms ($u < 0$), ordering proceeds locally by patches. This could explain the experimental observation of small B2 ordered domains in as-quenched Fe-Al alloys, in cases where phenomenological theories predict a congruent ordering [39].

Precipitation and ordering in Ni(Cr,Al) FCC alloys have been studied by Pareige *et al*. [21], with MC parameters fitted to thermodynamic and diffusion properties of Ni-rich solid solutions (Fig. 9a). For relatively small Cr and Al

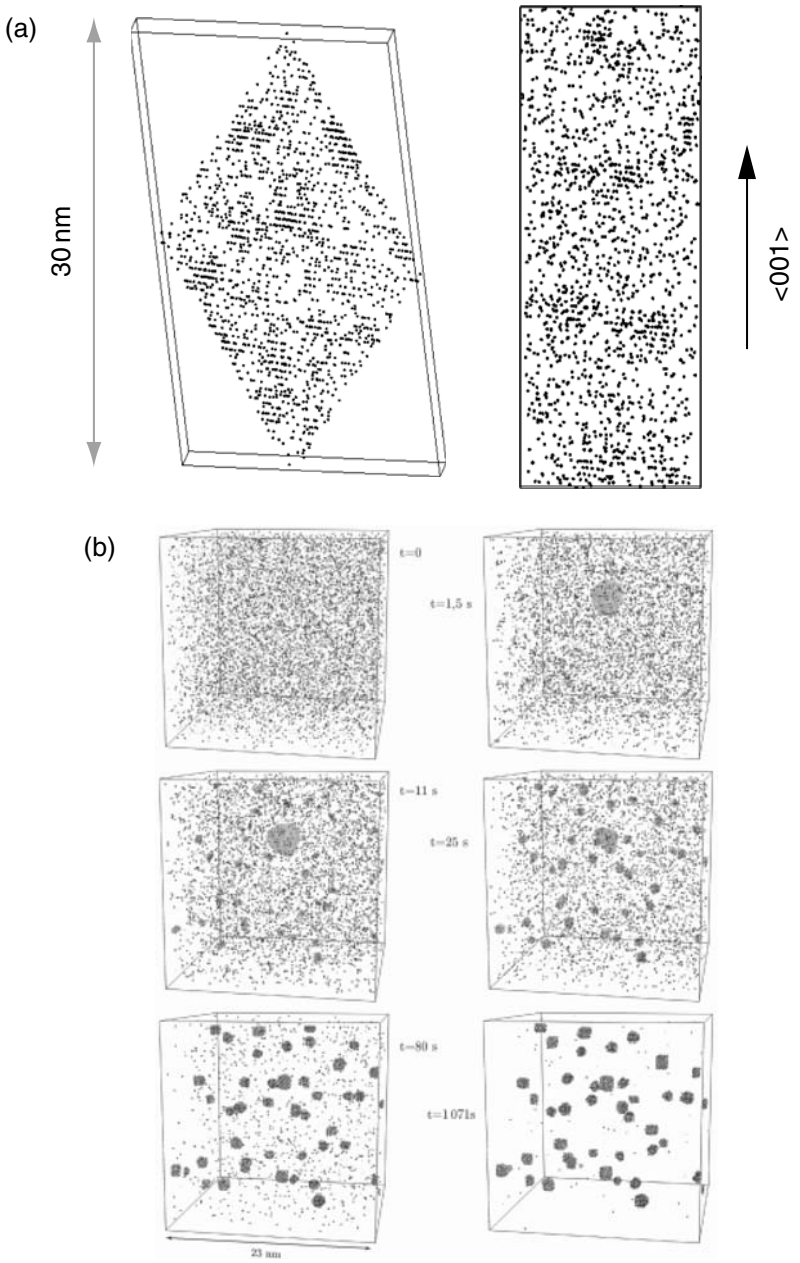

Figure 9. (a) Microstructure of a Ni-14.9at.%Cr-5.2at%Al alloy after a thermal ageing of 1 h at 600°C. Monte Carlo simulation (left) and 3D atom probe image (right). Each dot represents an Al atom (for the sake of clarity, Ni and Cr atoms are not represented). One observes the Al-rich 100 planes of γ' precipitates, with an average diameter of 2 nm [21]. (b) Monte Carlo simulation of NbC precipitation in ferrite with transient precipitation of a metastable iron carbide, shown in faint in the snapshots at 1.5, 11 and 25 seconds [28].

contents, at 873 K, the phase transformation occurs in three stages: (i) a short range ordering of the FCC solid solution, with two kinds of ordering symmetry (a "Ni_3Cr" symmetry corresponding to the one observed at high temperature in binary Ni–Cr alloys, and an $L1_2$ symmetry) followed by a nucleation-growth-coarsening sequence, (ii) the formation of the Al-rich γ' precipitates (with $L1_2$ structure), (iii) the growth and coarsening of the precipitates. In the γ' phase Cr atoms substitute for both Al and Ni atoms, with a preference for the Al sublattice. The simulated kinetics of precipitation are in good agreement with 3D-atom probe observations during a thermal ageing of the same alloy, at the same temperature [21]. For higher Cr and Al contents, MC simulations predict an congruent L12 ordering (with many small antiphase domains) followed by the $\gamma - \gamma'$ decomposition, as in the A2/B2 case discussed above.

4.5. Interstitial and Vacancy Diffusion in Parallel

Advanced high purity steels offer a field of application of KMC with practical relevance. In so called High-Strength Low-Alloy (HSLA) steels, Nb is used as a means to retain carbon in niobium carbide precipitates, out of solution in the BCC ferrite. The precipitation of NbC implies the migration, in the BCC Fe lattice, of both Nb, by vacancy mechanism, and C, by direct interstitial mechanism. At very early stages, the formation of coherent NbC clusters on the BCC iron lattice is documented from 3D atom probe observations.

The very same Monte Carlo technique can be used [28]; the new feature is the large value of the number of channels by which a configuration can decay, because of the many a priori possible jumps of the numerous carbon atoms. This makes step 3 of the algorithm above, very time consuming. A proper grouping of the channels, as a function of their respective decay time, helps speeding up this step. Among several interesting features, KMC simulations revealed the possibility for NbC nucleation to be preceded by the formation of a transient iron carbide, due to the rapid diffusion of C atoms by comparison with Nb and Fe diffusion (Fig. 9b). This latter kinetic pathway is found to be sensitive to the ability of the microstructure to provide the proper equilibrium vacancy concentration during the precipitation process.

4.6. Driven Alloys

KMC offers a unique tool to explore the stability and the evolution of the microstructure in "Driven Alloys", i.e., alloys exposed to a steady flow of energy, such as alloys under irradiation, or ball milling, or cyclic loading... [40]. Atoms in such alloys, change position as a function of time because of two mechanisms acting in parallel: one of the thermal diffusion mechanisms as discussed above, on the one hand, and forced, or "ballistic jumps"

on the other hand. The latter occur with a frequency imposed by the coupling with the surrounding of the system: their frequency is proportional to some "forcing intensity" (e.g., the irradiation flux). This situation is reminiscent of the "Kinetic Ising Model with two competing dynamics", much studied in the late 80s. However, one observes a strong sensitivity of the results to the details of the diffusion mechanism and of the ballistic jumps.

The main results are :

– a solubility limit which is a function both of the temperature and of the ratio of the frequencies of ballistic to thermally activated jumps (i.e., on the forcing intensity);
– at given temperature and forcing intensity, the solubility limit may also depend on the number of ballistic jumps to occur at once ("cascade size effect");
– the "replacement distance", i.e., the distance of ballistic jumps has a crucial effect on the phase diagrams as shown in Fig. 10. For appropriate replacement distances, self-patterning can occur, with a characteristic length, which depends on the forcing intensity and on the replacement distance [41].

What has been said of the solubility limit also applies to the kinetic pathways followed by the microstructure when the forcing conditions are changed.

Such KMC studies and the associated theoretical work helped to understand, for alloys under irradiation, the respective effects of the time and space structure of the elementary excitation, of the dose rate and of the integrated dose (or "fluence").

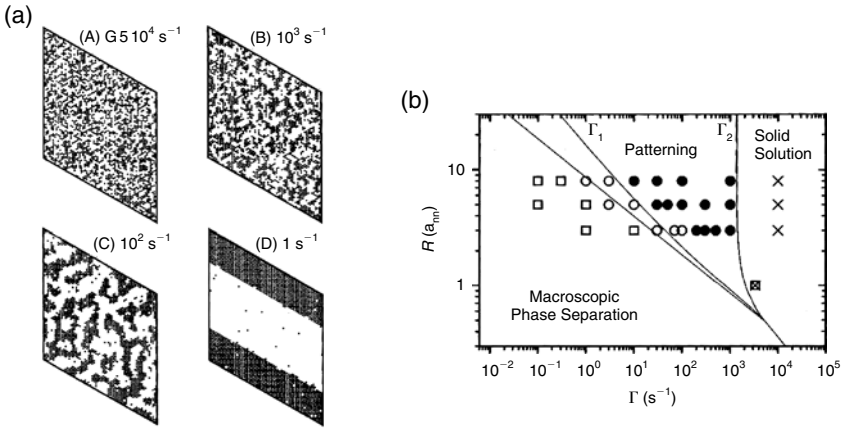

Figure 10. (a) Steady–state microstructures in KMC simulations of the phase separation in a binary alloy, for different ballistic jump frequencies Γ. (b) Dynamical phase diagram showing the steady–state microstructure as a function of the forcing intensity Γ and the replacement distance R [41].

5. Conclusion and Future Trends

The above presentation is by no means exhaustive. It aimed mainly at showing the necessity to model carefully the diffusion mechanism, and the techniques to do so, in order to have a realistic kinetic pathway for solid state transformations.

All the examples we gave are based on a rigid lattice description. The latter is correct as long as strain effects are not too large, as shown by the discussion of the Fe(Cu) alloy. Combining KMC for the configuration together with some technique to handle the relaxation of atomic positions is quite feasible, but for the time being requires a heavy computation cost if the details of the diffusion mechanism are to be retained. Interesting results have been obtained e.g., for the formation of strained hetero-epitaxial films [42].

A field of growing interest is the first principle determination of the parameters entering the transition probabilities. In view of the lack of experimental data for relevant systems, and of the fast improvement of such techniques, no doubt such calculations will be of extreme importance.

Finally, at the atomic scale, all the transitions modeled so far are either thermally activated or forced at some imposed frequency. A field of practical interest is where "stick and slip" type processes are operating: such is the case in shear transformations, in coherency loss etc. Incorporating such processes in KMC treatment of phase transformations has not yet been attempted to our knowledge, and certainly deserves attention.

Acknowledgments

We gratefully acknowledge many useful discussions with our colleagues at Saclay and at the Atom Probe Laboratory in the University of Rouen, as well as with Prs. Pascal Bellon (UICU) and David Seidman (NWU).

Appendix: The Kinetic Ising Model

In the KIM, the kinetic version of the model proposed by Ising for magnetic materials, the configurational Hamiltonian writes $H = \sum_{i \neq j} J_{ij} \sigma_i \sigma_j + \sum_i h_i \sigma_i$, with $\sigma_\iota = \pm 1$, the spin at site i, J_{ij}, the interaction parameter between spins at sites i and j, and h_i the external field on site i. The probability of a transition per unit time, between two configurations $\{\sigma_\iota\}$ and $\{\sigma'_\iota\}$ is chosen as: $W_{\{\sigma\},\{\sigma'\}} = w \exp[-(H' - H)/2k_B T]$, with w for the inverse time unit. Two models are studied:

KIM with conserved total spin, for which $\sum_i \sigma_i = \Sigma$ so that the configuration after the transition is obtained by permuting the spins on two (nearest neighbor) sites;

KIM with non-conserved total spin, for which the new configuration is obtained by flipping one spin on one given site.

When treated by Monte Carlo technique, two types of algorithms are currently applied to KIM:

Metropolis' algorithm, where the final configuration is accepted with probability one if $(H' - H) \leq 0$, and with probability $\exp[-(H' - H)/k_{\mathrm{B}}T]$ if $(H' - H) > 0$.

Glauber's algorithm, where the final configuration is accepted with probability $1/2\left[1 + \tanh(-(H' - H)/2k_{\mathrm{B}}T)\right]$.

References

[1] A.R. Allnatt and A.B. Lidiard, "Atomic transport in solids," Cambridge University Press, Cambridge, 1994.

[2] T. Morita, M. Suzuki, K. Wada, and M. Kaburagi, "Foundations and Applications of Cluster Variation Method and Path Probability Method," *Prog. Theor. Phys. Supp.*, 115, 1994.

[3] K. Binder, "Applications of Monte Carlo methods to statistical physics," *Rep. Prog. Phys.*, 60, 1997.

[4] Y. Limoge and J.-L. Bocquet, "Monte Carlo simulation in diffusion studies: time scale problems," *Acta Met.*, 36, 1717, 1988.

[5] G.E. Murch and L. Zhang, "Monte Carlo simulations of diffusion in solids: some recent developments," In: A.L. Laskar *et al*. (eds.), *Diffusion in Materials*, Kluwer Academic Publishers, Dordrecht, 1990.

[6] C.P. Flynn, "Point defects and diffusion," Clarendon Press, Oxford, 1972.

[7] J. Philibert, "Atom movements, diffusion and mass transport in solids," Les Editions de Physique, Les Ulis, 1991.

[8] D.N. Seidman and R.W. Balluffi, "Dislocations as sources and sinks for point defects in metals," In: R.R. Hasiguti (ed.), *Lattice Defects and their Interactions*, Gordon-Breach, New York, 1968.

[9] J.-L. Bocquet, G. Brebec, and Y. Limoge, "Diffusion in metals and alloys," In: R.W. Cahn and P. Haasen (eds.), *Physical Metallurgy*, North-Holland, Amsterdam, 1996.

[10] M. Nastar, V.Y. Dobretsov, and G. Martin, "Self consistent formulation of configurational kinetics close to the equilibrium: the phenomenological coefficients for diffusion in crystalline solids," *Philos. Mag. A*, 80, 155, 2000.

[11] G. Martin, "The theories of unmixing kinetics of solids solutions," In: *Solid State Phase Transformation in Metals and Alloys*, pp. 337–406. Les Editions de Physique, Orsay, 1978.

[12] A. Perini, G. Jacucci, and G. Martin, "Interfacial contribution to cluster free energy," *Surf. Sci.*, 144, 53, 1984.

[13] T.R. Waite, "Theoretical treatment of the kinetics of diffusion-limited reactions," *Phys. Rev.*, 107, 463–470, 1957.

[14] I.M. Lifshitz and V.V. Slyosov, "The kinetics of precipitation from supersaturated solid solutions," *Phys. Chem. Solids*, 19, 35, 1961.

[15] C.J. Kuehmann and P.W. Voorhees, "Ostwald ripening in ternary alloys," *Metall. Mater Trans.*, 27A, 937–943, 1996.

[16] J.W. Cahn, W. Craig Carter, and W.C. Johnson (eds.), The selected works of J.W. Cahn., TMS, Warrendale, 1998.
[17] G. Martin, "Atomic mobility in Cahn's diffusion model," *Phys. Rev. B*, 41, 2279–2283, 1990.
[18] C. Desgranges, F. Defoort, S. Poissonnet, and G. Martin, "Interdiffusion in concentrated quartenary Ag–In–Cd–Sn alloys: modelling and measurements," *Defect Diffus. For.*, 143, 603–608, 1997.
[19] S.M. Allen and J.W. Cahn, "A macroscopic theory for antiphase boundary motion and its application to antiphase domain coarsening," *Acta Metal.*, 27, 1085–1095, 1979.
[20] P. Bellon and G. Martin, "Coupled relaxation of concentration and order fields in the linear regime," *Phys. Rev. B*, 66, 184208, 2002.
[21] C. Pareige, F. Soisson, G. Martin, and D. Blavette, "Ordering and phase separation in Ni–Cr–Al: Monte Carlo simulations vs Three-Dimensional atom probe," *Acta Mater.*, 47, 1889–1899, 1999.
[22] Y. Le Bouar and F. Soisson, "Kinetic pathways from EAM potentials: influence of the activation barriers," *Phys. Rev. B*, 65, 094103, 2002.
[23] E. Clouet and N. Nastar, "Monte Carlo study of the precipitation of Al_3Zr in Al–Zr," *Proceedings of the Third International Alloy Conference*, Lisbon, in press, 2002.
[24] J.-L. Bocquet, "On the fly evaluation of diffusional parameters during a Monte Carlo simulation of diffusion in alloys: a challenge," *Defect Diffus. For.*, 203–205, 81–112, 2002.
[25] R. LeSar, R. Najafabadi, and D.J. Srolovitz, "Finite-temperature defect properties from free-energy minimization," *Phys. Rev. Lett.*, 63, 624–627, 1989.
[26] A.P. Sutton, "Temperature-dependent interatomic forces," *Philos. Mag.*, 60, 147–159, 1989.
[27] Y. Mishin, M.R. Sorensen, F. Arthur, and A.F. Voter, "Calculation of point-defect entropy in metals," *Philos. Mag. A*, 81, 2591–2612, 2001.
[28] D. Gendt, Cinétiques de Précipitation du Carbure de Niobium dans la ferrite, CEA Report, 0429–3460, 2001.
[29] M. Athènes, P. Bellon, and G. Martin, "Identification of novel diffusion cycles in B2 ordered phases by Monte Carlo simulations," *Philos. Mag. A*, 76, 565–585, 1997.
[30] M. Athènes and P. Bellon, "Antisite diffusion in the L12 ordered structure studied by Monte Carlo simulations," *Philos. Mag. A*, 79, 2243–2257, 1999.
[31] A. Athènes, P. Bellon, and G. Martin, "Effects of atomic mobilities on phase separation kinetics: a Monte Carlo study," *Acta Mater.*, 48, 2675, 2000.
[32] R. Wagner and R. Kampmann, "Homogeneous second phase precipitation," In: P. Haasen (ed.), *Phase Transformations in Materials*, VCH, Weinhem, 1991.
[33] F. Soisson, A. Barbu, and G. Martin, "Monte Carlo simulations of copper precipitation in dilute iron-copper alloys during thermal ageing and under electron irradiation," *Acta Mater.*, 44, 3789, 1996.
[34] P. Auger, P. Pareige, M. Akamatsu, and D. Blavette, "APFIM investigation of clustering in neutron irradiated Fe–Cu alloys and pressure vessel steels," *J. Nucl. Mater.*, 225, 225–230, 1995.
[35] P. Fratzl and O. Penrose, "Kinetics of spinodal decomposition in the Ising model with vacancy diffusion," *Phys. Rev. B*, 50, 3477–3480, 1994.
[36] J.-M. Roussel and P. Bellon, "Vacancy-assisted phase separation with asymmetric atomic mobility: coarsening rates, precipitate composition and morphology," *Phys. Rev. B*, 63, 184114, 2001.
[37] F. Soisson and G. Martin, *Phys. Rev. B*, 62, 203, 2000.

[38] E. Clouet, M. Nastar, and C. Sigli, "Nucleation of Al_3Zr and Al_3Sc in aluminiun alloys: from kinetic Monte Carlo simulations to classical theory," *Phys. Rev. B*, 69, 064109, 2004.
[39] M. Athènes, P. Bellon, G. Martin, and F. Haider, "A Monte Carlo study of B2 ordering and precipitation via vacancy mechanism in BCC lattices," *Acta Mater.*, 44, 4739–4748, 1996.
[40] G. Martin and P. Bellon, "Driven alloys," *Solid State Phys.*, 50, 189, 1997.
[41] R.A. Enrique and P. Bellon, "Compositional patterning in immiscible alloys driven by irradiation," *Phys. Rev. B*, 63, 134111, 2001.
[42] C.H. Lam, C.K. Lee, and L.M. Sander, "Competing roughening mechanisms in strained heteroepitaxy: a fast kinetic Monte Carlo study," *Phys. Rev. Lett.*, 89, 216102, 2002.